Grain-Boundary Character Distribution in Recrystallized $L1_2$ Ordered Intermetallic Alloys

Y. KANENO and T. TAKASUGI

The grain-boundary character distribution (GBCD) of cold-rolled and, subsequently, recrystallized Co_3Ti and $Ni_3(Si,Ti)$ ordered alloys with an $L1_2$ structure was studied by the electron backscattered diffraction (EBSD) method, in association with texture. For comparison, the GBCD of recrystallized pure copper and aluminum was also determined. The recrystallization textures of the Co_3Ti alloys as well as the $Ni_3(Si,Ti)$ alloy were significantly weak and different from those of the pure copper and aluminum with a strong cube texture. The GBCD of the Co_3Ti alloys was characterized by a high frequency of $\Sigma 3$ boundaries. On the other hand, the GBCD of the $Ni_3(Si,Ti)$ alloy was characterized by a lower frequency of $\Sigma 3$ and higher frequency of random (*e.g.*, $\Sigma > 29$) boundaries than that of the Co_3Ti alloys. However, the GBCDs of the Co_3Ti and $Ni_3(Si,Ti)$ alloys were similar to each other and also quite similar to those of the pure copper and aluminum, when $\Sigma 3$ boundaries are excluded from the GBCD. Based on these results, the formation mechanism responsible for the recrystallization textures and the grain-boundary structure and energy of the Co_3Ti and $Ni_3(Si,Ti)$ alloys were discussed, in comparison with those of pure copper and aluminum.

I. INTRODUCTION

THE grain boundary is one of the important metallurgical factors affecting the mechanical, physical, and chemical properties of polycrystalline materials. The grain-boundary structure is often evaluated using a Σ value, which is defined based on the coincidence-site lattice (CSL) theory.[1] It is well known that grain-boundary properties are strongly dependent on the type and structure of grain boundaries[1] and also that low-Σ boundaries show high resistance to fracture[2,3] and corrosion.[1,4] Therefore, the grain-boundary character distribution (GBCD) is considered to be a factor used for improving properties of polycrystalline materials. Recent studies concerning the grain-boundary structure focus on the relationship between the GBCD and (crystallographic) texture,[5–10] because most engineering metallic materials, which are usually produced by thermomechanical processing, are textured to a greater or less extent. For instance, the GBCD of conventional metals and alloys such as aluminum,[11,12]. nickel,[13,14] copper,[15,16,17] and iron[18] has been investigated in association with texture.

More recently, much attention has been paid to the GBCD of ordered intermetallic alloys. Many ordered intermetallic alloys show high strength, good corrosion resistance, and high phase stability, which make them attractive candidate structural materials for applications at elevated temperatures. However, the room-temperature ductility of ordered intermetallic alloys is generally low because of their complex crystal structures. By extensive efforts carried out during the past two decades, the tensile ductility of $L1_2$ ordered intermetallic alloys, which have suffered from a propensity for intergranular fracture, was improved by micro- and macroalloying,[19,20,21] and, consequently, fairly good ductility at low temperatures was achieved. In fact, boron-doped Ni_3Al,[22–27] Co_3Ti,[28,29,30] and $Ni_3(Si,Ti)$[31,32,33] can be plastically deformed at room temperature. It has also been reported that boron-free binary Ni_3Al with a unidirectionally solidified structure could be heavily cold rolled to thin foil.[34] For these ductile (deformable) intermetallic alloys, microstructure control for grain size and texture is possible by thermomechanical processing. It is, therefore, necessary to understand the fundamental phenomena of the recrystallization, such as the microstructure, texture, and grain-boundary structure (*i.e.*, the GBCD) of the intermetallic alloys. Also, the control of the GBCD is expected to lead to further improvement and optimization of the properties of intermetallic alloys. For intermetallic alloys, the GBCD of $L1_2$-type Ni_3Al[35–39] and B2-type FeAl[40,41,42] and NiAl[42] has been investigated, but the GBCD of $L1_2$-type Co_3Ti and $Ni_3(Si,Ti)$ alloys has not been studied so far. It is known that both the Co_3Ti[20] and $Ni_3(Si,Ti)$[21] alloys show a positive temperature dependence of yield strength and also have a stable $L1_2$ phase up to their melting point.

In the previous study, the texture development during cold rolling and recrystallization of $L1_2$-type Co_3Ti[30] and $Ni_3(Si,Ti)$[33] alloys was investigated by the present authors. The present study addresses the GBCD of the cold-rolled and recrystallized Co_3Ti and $Ni_3(Si,Ti)$ alloys in association with texture. The influence of alloy type, off-stoichiometry, and cold-rolling reduction is examined. Moreover, to deeply evaluate the nature of the GBCD in ordered intermetallic alloys, the GBCD of the cold-rolled and recrystallized pure copper and aluminum, which have medium and high stacking fault energies (SFEs), respectively, was also determined to provide typical examples of disordered (fcc) materials with strong recrystallization texture. Additionally, by using pure metals, the effect of wrong bonds at the grain boundary for ordered intermetallic alloys can be considered clearly, because wrong bonds are completely absent in pure metals. Some data obtained in the previous studies[30,33] were incorporated into this study.

Y. KANENO, Research Associate, and T. TAKASUGI, Professor, are with Department of Metallurgy and Materials Science, Graduate School of Engineering, Osaka Prefecture University, Osaka 599-8531, Japan. Contact e-mail: kaneno@mtl.osakafu-u.ac.jp

Manuscript submitted December 30, 2002.

II. EXPERIMENTAL PROCEDURES

Materials used in this study were two Co_3Ti alloys and a $Ni_3(Si,Ti)$ alloy. Nominal compositions of the alloys used were $Co_{78}Ti_{22}$, $Co_{77}Ti_{23}$, and $Ni_{79}Si_{11}$ Ti_{10} doped with 50 ppm boron (denoted by at. pct), respectively. In the present article, only the results for the $Co_{77}Ti_{23}$ alloy are presented, because the majority of experimental results for the $Co_{78}Ti_{22}$ alloy were similar to those for the $Co_{77}Ti_{23}$ alloy. These alloys were prepared by arc melting in an argon gas atmosphere on a copper hearth using a nonconsumable tungsten electrode. The purity of each raw material was over 99.9 wt pct. Homogenization heat treatment was conducted in a vacuum at 1323 K for 48 hours, followed by furnace cooling. Homogenized ingots were rolled in air at 773 K for the Co_3Ti alloys and at 573 K for the $Ni_3(Si,Ti)$ alloy and then annealed at 1273 K for 5 hours. This procedure was repeated several times until a desired thickness (~4 mm) was obtained. The rolled ingots were finally annealed at 1273 K for 5 hours to prepare starting materials for cold rolling. Cold rolling was conducted up to ~70 to 80 pct reduction. Finally, the cold-rolled sheets were annealed at 1273 K for 1 hour for the Co_3Ti alloys and at 1173 K for 1 hour for the $Ni_3(Si,Ti)$ alloy, respectively. For comparison, fully recrystallized oxygen-free copper (99.9 mass pct Cu) and a commercial AA1070 aluminum (99.78 mass pct Al) were cold rolled to 90 pct reduction and, subsequently, recrystallized in a salt bath at 673 K for copper and at 773 K for aluminum, respectively. For macrotexture, conventional X-ray pole figures were measured using samples with a size of $\sim 20 \times 20$ mm^2. From the measured incomplete pole figures, the complete orientation distribution functions (ODFs), including odd terms for ghost correction, were determined by the iterative series-expansion method. For microtexture including grain-boundary structure, local orientations were measured by the electron backscattered diffraction (EBSD) technique using the same samples as those for the X-ray pole-figure measurement. Typically, an area of $\sim 200 \times 200$ μm^2 was scanned with a step size of ~1.6 μm (or ~1.3 μm), and a total of ~55,000 (or ~220,000) points were analyzed using the INCA CRYSTAL* software developed by OXFORD INSTRUMENTS. The Brandon criterion,[43] $\Delta\theta_{max} = 15 \text{ deg } \Sigma^{-1/2}$, was used to classify the grain-boundary character in terms of the CSL model.

*INCA CRYSTAL and OXFORD INSTRUMENTS are trademarks of Oxford Instruments, United Kingdom.

III. RESULTS

A. *Optical Microstructures*

Typical microstructures of recrystallized materials are shown in Figures 1(a) through (d). The Co-23Ti alloy exhibits a fully recrystallized microstructure consisting of $L1_2$ equiaxed grains (Figure 1(a)). The grain sizes of the recrystallized Co-23Ti alloy are almost identical, irrespective of cold-rolling reduction. Microstructural features of the Co-22Ti alloy are identical to those of the Co-23Ti alloy. Also, the $Ni_3(Si,Ti)$ alloy shows a fully recrystallized microstructure consisting of $L1_2$ equiaxed grains (Figure 1(b)). Annealing twins are observed in the recrystallized microstructures of both the Co_3Ti and $Ni_3(Si,Ti)$ alloys, but are apparently more significant in the Co_3Ti alloy than in the $Ni_3(Si,Ti)$ alloy. For the 90 pct cold-rolled copper sheet, annealing at 673 K results in a fully recrystallized microstructure for the investigated annealing time. Many annealing twins are observed in the recrystallized copper (Figure 1(c)) as well as in the Co_3Ti alloy. For the 90 pct cold-rolled aluminum, coarse recrystallized grains are formed by annealing at 773 K for 10 ks (Figure 1(d)).

B. *Macrotextures*

Figures 2(a) through (d) show a typical example of a {111} pole figure by X-ray diffraction for each recrystallized material. The previous study has demonstrated that the recrystallization textures of the Co-22Ti and Co-23Ti (Figure 2(a)) alloys are similar to each other, and that no remarkable difference can be observed in the two Co_3Ti alloys, irrespective of rolling reduction (*i.e.*, 30, 50, and 70 pct reductions).[30] On the other hand, the recrystallization texture of the $Ni_3(Si,Ti)$ alloy (Figure 2(b)) is quite different from that of the Co_3Ti alloys. Also, it is noted that the recrystallization textures of both the $Ni_3(Si,Ti)$ and Co_3Ti alloys are weak. In the $Ni_3(Si,Ti)$ alloy, the recrystallization texture of the 30 pct cold-rolled sheet is somewhat different from the recrystallization textures of the 50, 70, and 80 pct cold-rolled sheets: the 30 pct cold-rolled sheet exhibits a recrystallization texture similar to its rolling texture.[33] The details for the cold rolling and recrystallization textures of the Co_3Ti and $Ni_3(Si,Ti)$ alloys are described elsewhere (References 30 and 33). By contrast, a quite different texture, that is, a strong {001} <100> cube texture, is formed both in copper (Figure 2(c)) and aluminum (Figure 2(d)). A cube texture is well known to be formed in the heavily rolled and subsequently annealed fcc materials with medium and high stacking fault energies (*e.g.*, References 44 through 47).

Figures 3(a) and (b) show the φ_2 sections of the ODFs for the recrystallized materials. Some ideal orientations observed in the present materials are also included in this figure ({001}<110> and {001}<130> orientations are illustrated only in the $\varphi_2 = 0$, 45, and 90 deg sections). For the Co-23Ti alloy (Figure 3(a)), the recrystallization textures of the 70 pct cold-rolled sheets are quite weak and accompanied by an extensive orientation spread, but {112}<111> and {011}<100> orientations, which are main components of the rolling texture, are still found. For the 70 pct cold-rolled $Ni_3(Si,Ti)$ alloy sheet (Figure 3(b)), the recrystallization texture is similarly weak, but {001}<110> and {011}<100> orientations can be found. On the other hand, very strong recrystallization textures are again recognized in the copper and aluminum sheets in comparison with the Co_3Ti and $Ni_3(Si,Ti)$ alloys, although the rolling reduction for copper and aluminum is somewhat larger than that for the Co_3Ti and $Ni_3(Si,Ti)$ alloys. The {001}<100> cube orientation is a main component in the recrystallization textures of both copper and aluminum, but minor components are different between the two materials. A minor component of the {122}<221> orientation, which has a twin relationship with a {001}<100> cube orientation,[44–47] is observed for copper, while {112}<132> and {123}<634> orientations are observed for aluminum. In the case of aluminum,

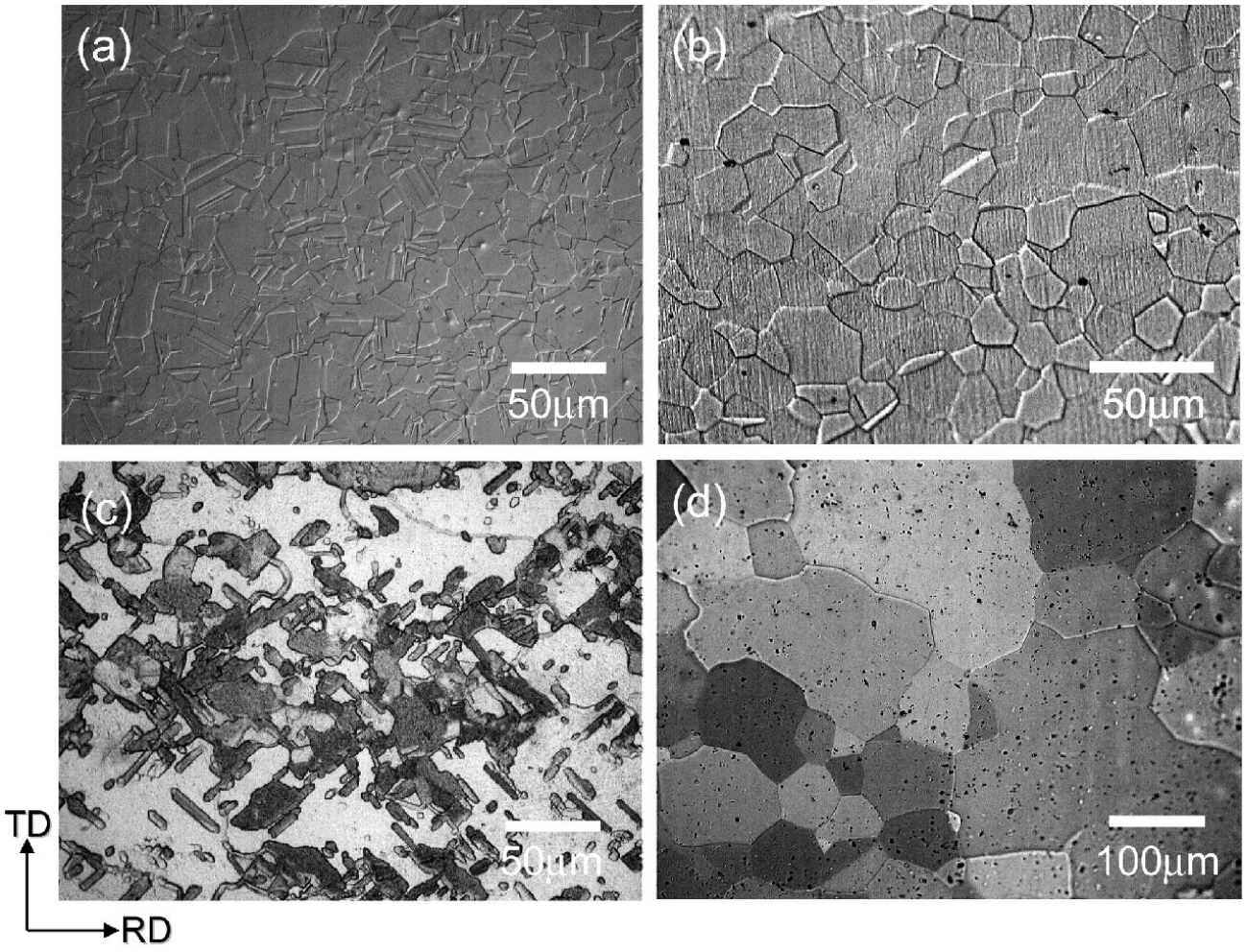

Fig. 1—Optical micrographs of (*a*) Co-23 Ti that was cold rolled to 70 pct reduction and subsequently annealed at 1273 K for 1 h, (*b*) $Ni_3(Si,Ti)$ that was cold rolled to 70 pct reduction and subsequently annealed at 973 K for 1 h, (*c*) copper that was cold rolled to 90 pct reduction and subsequently annealed at 673 K for 2 h, and (*d*) aluminum that was cold rolled to 90 pct reduction and subsequently annealed at 773 K for 10 ks (RD: rolling direction, and TD: transverse direction).

the formation of these orientations has been suggested to be due to the minor elements such as iron and silicon.[49,50] The orientation density of the {001}<100> cube orientation is significantly higher in copper than in aluminum. These results of the macrotexture clearly indicate that the recrystallization textures of the cold-rolled ordered intermetallic alloys (*i.e.*, the Co_3Ti and $Ni_3(Si,Ti)$ alloys) are much weaker than those of the cold-rolled disordered metals (*i.e.*, copper and aluminum).

C. *Microtextures*

Figures 4(a) through (d) show {111} pole figures of recrystallized materials obtained by the EBSD technique. In these figures, orientations of approximately 500 to 600 grains (including annealing twins) were mostly measured. Generally, the scanned area in the EBSD measurement is much smaller than the irradiation area in the X-ray diffraction measurement. Consequently, the pole figures obtained by the EBSD technique are sometimes ambiguous in comparison with that obtained by the X-ray diffraction. Nevertheless, for the Co_3Ti and $Ni_3(Si,Ti)$ alloys (Figures 4(a) and (b)), the distribution of the grain orientation in the EBSD pole figures seems to be consistent with that in the X-ray pole figures (Figures 2(a) and (b)). For copper and aluminum (Figures 4(c) and (d)), the EBSD pole figures are in good agreement with the X-ray pole figures (Figures 2(c) and (d)).

D. *Grain-Boundary Structures*

Figures 5(a) through (d) the typical distribution of grain-boundary misorientation angle for recrystallized materials. For the Co-23Ti alloy (Figure 5(a)), a significant occurrence (frequency) is found at the misorientation angle of ~60 deg. The frequency at the misorientation angle of ~60 deg is found to be lower in the $Ni_3(Si,Ti)$ alloy (Figure 5(b)) than in the Co-23Ti alloy. Additionally, a greater occurrence of the low-angle ($\theta \leq 15$ deg) boundaries is observed in the $Ni_3(Si,Ti)$ alloy, and, with the exception of the high frequency at ~60 deg, the misorientation distribution of the $Ni_3(Si,Ti)$ alloy is similar to that of randomly oriented materials.[51] The high frequency of grain-boundary misorientation at the misorientation angle of ~60 deg is also found for copper (Figure 5(c)). In addition, the distribution of the low-angle ($\theta \leq 15$ deg) boundaries seems to be relatively high for copper. However, such a distinctive occurrence at the

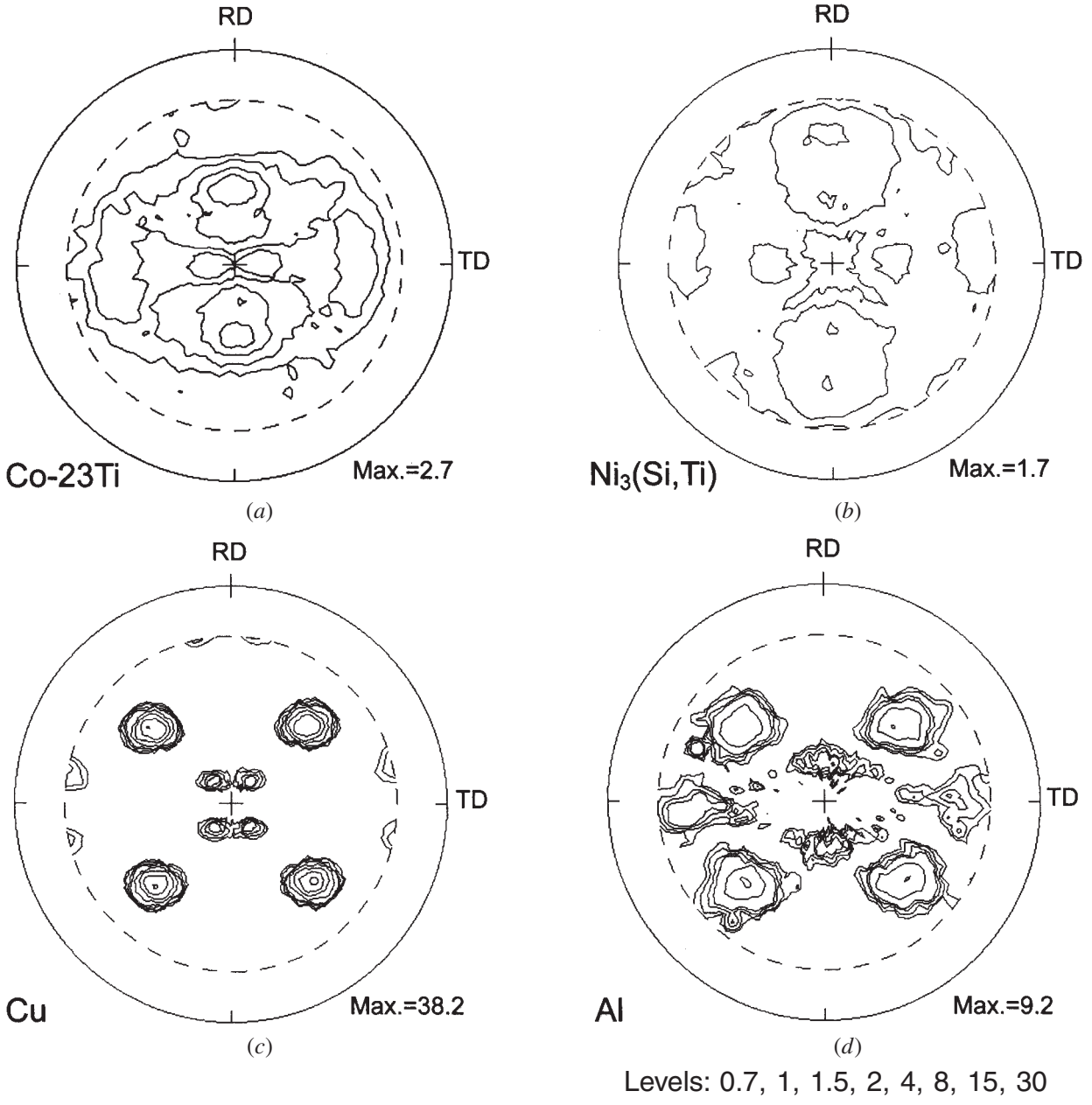

Fig. 2—{111} pole figures of (*a*) Co-23 Ti, (*b*) $Ni_3(Si,Ti)$, (*c*) copper, and (*d*) aluminum. The annealing condition of each specimen except (c) copper that was cold rolled to 90 pct reduction and subsequently annealed at 673 k for 24 h, is the same as that shown in Fig. 1.

misorientation angle of ~60 deg is not found for aluminum, as shown in Figure 5(d).

A typical GBCD for recrystallized materials is shown in Figures 6(a) through (d). The GBCD of the Co-23Ti alloy (Figure 6(a)) is primarily featured by the high frequency of $\Sigma 3$ boundaries. This high frequency of $\Sigma 3$ boundaries corresponds to a high frequency of the grain-boundary misorientation at the misorientation angle of ~60 deg, because $\Sigma 3$ boundaries have a 60 deg/<111> relationship.[1] Also, a low but recognizable frequency is observed for $\Sigma 1$ and $\Sigma 9$ boundaries. The occurrence of $\Sigma 9$ boundaries (and also $\Sigma 27$ boundaries), *i.e.*, $\Sigma 3^n$ boundaries, may be due to geometric interactions of twin-related variants.[52] However, the occurrence of other special boundaries (*i.e.*, $\Sigma \leq 29$) is very low in the Co-23Ti alloy. No remarkable difference in the GBCD is found between the Co-22Ti and Co-23Ti alloys. These results suggest that off-stoichiometry in the Co_3Ti alloys little affects the GBCD, as well as the grain size and texture of the recrystallized specimen.[30] The GBCD of the $Ni_3(Si,Ti)$ alloy (Figure 6(b)) is featured by a lower frequency of $\Sigma 3$ boundaries and higher frequency of random (*e.g.*, $\Sigma \geq 29$) and $\Sigma 1$ boundaries than that of the Co-23Ti alloy. On the other hand, the GBCD of copper (Figure 6(c)) is analogous to that of the Co_3Ti alloy, except for the frequency of $\Sigma 1$ and random (*e.g.*, $\Sigma \geq 29$) boundaries: a higher frequency of $\Sigma 1$ boundaries and a lower frequency of random boundaries are observed in copper than in the Co_3Ti alloy. In aluminum, no remarkable special boundaries except for $\Sigma 1$ boundaries are observed, and the highest frequency of random boundaries is observed among all the materials used in this study (Figure 6(d)).

Based on the Σ value of the grain boundaries, the type of grain boundary is divided into four classes as follows: (1) low-angle boundaries (LABs), characterized by Σ1; (2) twin boundaries and related boundaries, characterized by $\Sigma 3^n$; (3) other special boundaries, characterized by Σ5, Σ7, Σ11 to Σ25, Σ29; and (4) random boundaries,

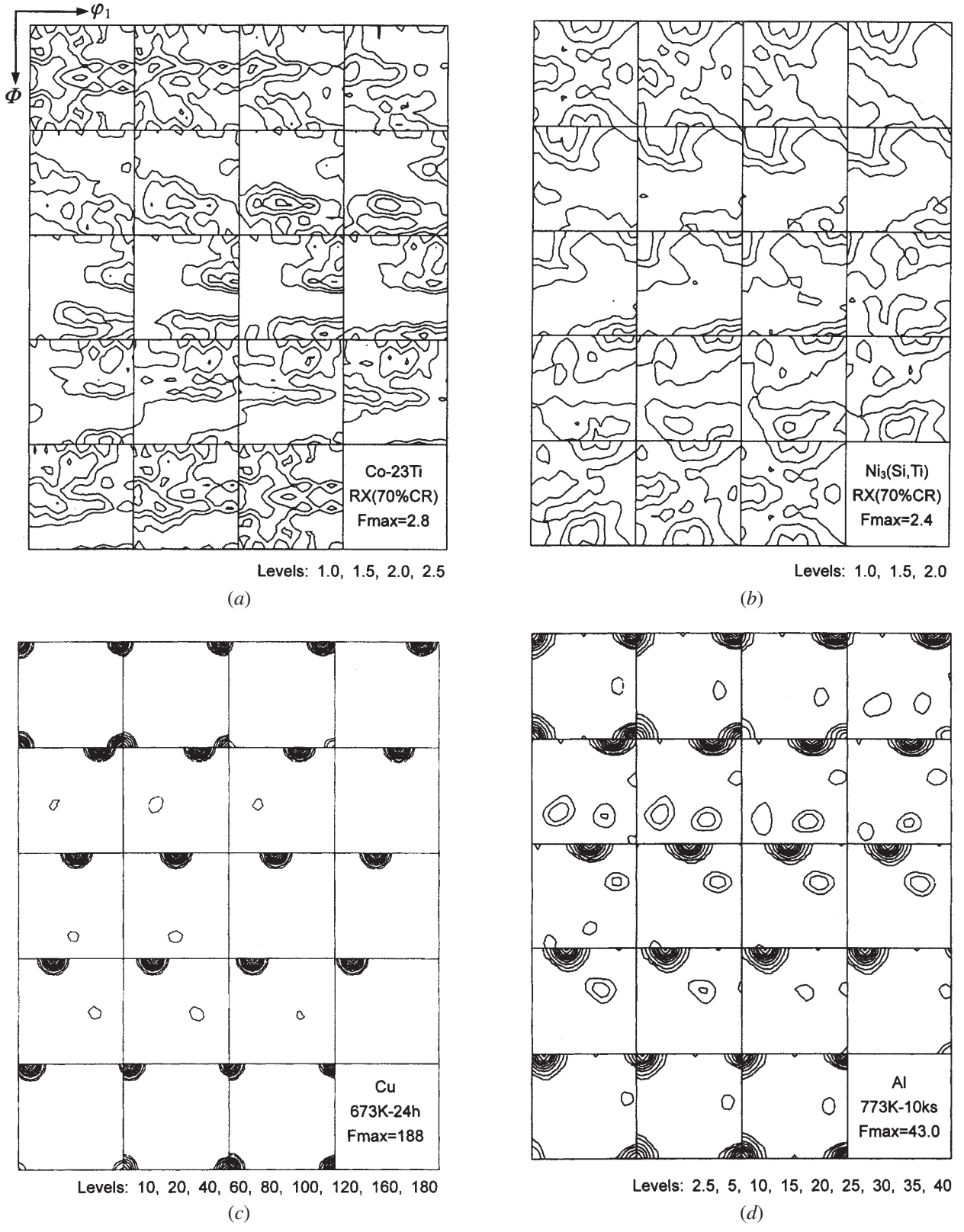

Fig. 3—The φ_2 sections of the ODFs for the (*a*) Co-23 Ti, (*b*) Ni_3(Si,Ti), (*c*) copper, and (*d*) aluminum. The annealing condition of each specimen is the same as that shown in Fig. 2. Some ideal orientations in Euler angle space are shown in (e).

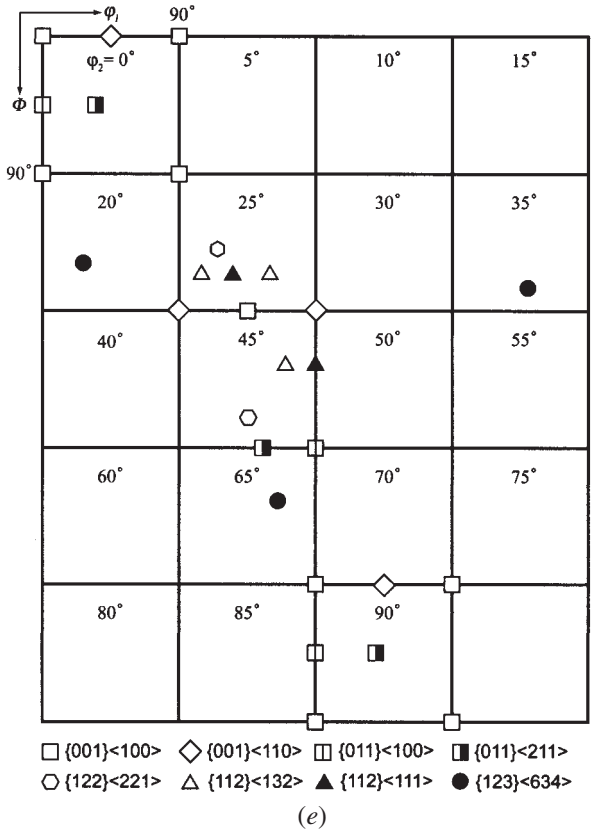

(*e*)

Fig. 3—Continued. The φ_2 sections of the ODFs for the (*a*) Co-23 Ti, (*b*) $Ni_3(Si,Ti)$, (*c*) copper, and (*d*) aluminum. The annealing condition of each specimen is the same as that shown in Fig. 2. Some ideal orientations in Euler angle space are shown in (e)

characterized by $\Sigma > 29$. The classified grain boundaries for recrystallized materials are summarized in Table I. From Table I and Figures 6(a) through (d), it is found that the GBCD of the Co-23Ti alloy is analogous to that of copper, while the GBCD of the $Ni_3(Si,Ti)$ alloy is similar to that of aluminum, except for the $\Sigma 3$ boundaries. Although the frequency of $\Sigma 3$ boundaries (as well as $\Sigma 1$ boundaries (LABs)) somewhat varies, depending on cold-rolling reduction or annealing time, it can be ranked as of the order $Co_3Ti \geq Cu > Ni_3(Si,Ti) > Al$. However, Table I also indicates that the frequency of twin-related boundaries (*i.e.*, the $\Sigma 9$ and $\Sigma 27$ boundaries) is generally higher in copper than in the Co_3Ti alloys, although it tends to decrease with increasing annealing time for copper.

Figure 7 shows EBSD boundary maps for the recrystallized Co_3Ti (Co-23Ti) alloy and copper. In this figure, $\Sigma 3$ boundaries are colored as yellow. These figures clearly indicate that twin ($\Sigma 3$) boundaries of the Co_3Ti alloy are quite straight and relatively long (in most cases, twin boundaries exist across the entire grain, *i.e.*, as *transgrain (perfect)* twin boundaries) while those of copper exist in the form of *islandlike (imperfect)* annealing twins. In other words, twin boundaries of the Co_3Ti alloys are mostly composed of *coherent* planes, while those of copper are composed of not only coherent planes but also *incoherent* planes. Also, the $Ni_3(Si,Ti)$ alloy shows a similar twin-boundary morphology to that of the Co-23Ti alloy.

IV. DISCUSSION

A. *Mechanisms for Recrystallization Textures in $L1_2$ Ordered Intermetallic Alloys*

It is first pointed out that, basically, the GBCD of the recrystallized Co_3Ti and $Ni_3(Si,Ti)$ alloys is analogous to that of the recrystallized disordered materials (*i.e.*, copper and aluminum), although the recrystallization textures of the Co_3Ti and $Ni_3(Si,Ti)$ alloys are considerably different from the strong cube recrystallization textures of copper and aluminum. This implies that the type and intensity of textures are not the prime factors governing the GBCD of the recrystallized materials, or, otherwise, the GBCD of the recrystallized materials is not correlated with the type and intensity of textures.

Here, we discuss the formation mechanism for recrystallization textures of the Co_3Ti and $Ni_3(Si,Ti)$ alloys. Weak recrystallization textures appear to be characteristic of recrystallized $L1_2$-type ordered intermetallic alloys, as have been actually observed in Cu_3Au,[53] boron-doped Ni_3Al,[22,24–26] Co_3Ti,[30] and $Ni_3(Si,Ti)$[33] alloys. Although the formation mechanisms responsible for such weak recrystallization textures in $L1_2$-type ordered intermetallic alloys are unclear at the moment, some possible reasons are suggested. First, it is very likely that the weak deformation textures are followed by weak recrystallization textures. In fact, weak deformation textures have been repeatedly reported in cold-rolled $L1_2$-type ordered intermetallic alloys such as Cu_3Au[53] and boron-doped Ni_3Al,[22,24–26] as well as in the Co_3Ti[30] and $Ni_3(Si,Ti)$[33] alloys. Second, inhomogeneous deformation microstructure such as shear bands, which have been often observed for these ordered intermetallic alloys,[23,26,27,29,33] may be associated with the weak recrystallization textures. It has been widely accepted that inhomogeneous deformation interferes with the development of recrystallization texture and, consequently, weakens the recrystallization texture.[54] Third, the origin of the weak recrystallization texture in $L1_2$-type ordered intermetallic alloys may be attributed to the specific nucleation process of recrystallization. It is generally accepted that recrystallization texture is developed through two fundamental processes, *i.e.*, the formation process of new nuclei of recrystallization and their growth process. In this study, it was observed that the GBCD of the recrystallized Co_3Ti and $Ni_3(Si,Ti)$ alloys is essentially the same as that of copper and aluminum with a strong recrystallization texture. This suggests that the growth process during recrystallization is not so different between the ordered intermetallic alloys and disordered materials. The primary recrystallization (or nucleation) process of recrystallization in cold-rolled $L1_2$-type ordered intermetallic alloys appears to be complicated and different from disordered fcc materials. Recovery, *i.e.*, dislocation rearrangement (polygonization), is assumed to be not easy, because dislocations in $L1_2$-type ordered intermetallic alloys are dissociated and, consequently, their glide and climb motions are slow. The primary recrystallization process of $L1_2$-type ordered intermetallic alloys involves structural and chemical reordering, because the degree of ordering is substantially reduced by the cold rolling. Therefore, it appears that the primary recrystallization process is retarded in $L1_2$-type ordered intermetallic alloys. The migration of grain boundaries in $L1_2$-type ordered intermetallic alloys is also assumed to be low because the grain boundaries have to

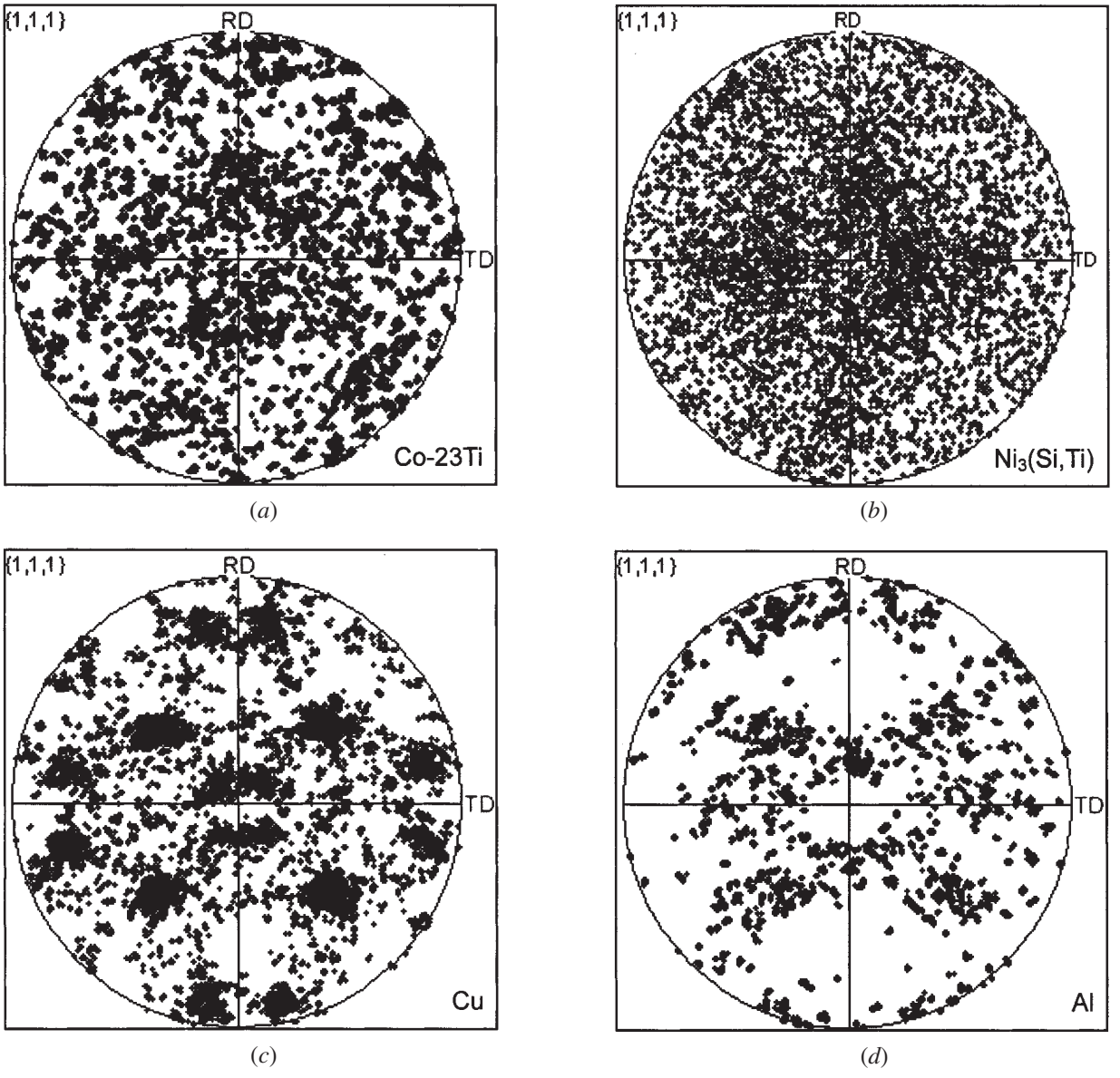

Fig. 4—EBSD {111} pole figures of the (*a*) Co-23 Ti, (*b*) $Ni_3(Si,Ti)$, (*c*) copper, and (*d*) aluminum. The annealing condition of each specimen is the same as that shown in Fig. 2.

migrate, keeping or restoring atomic ordering. Even if nuclei of recrystallization such as cube-orientated nuclei are formed in $L1_2$-type ordered intermetallic alloys, they cannot preferentially grow. Consequently, variously orientated grains will grow, resulting in a weak recrystallization texture. In addition, multiple twinning may be partly responsible for the weak recrystallization textures, particularly in the Co_3Ti alloys. However, to clarify the formation mechanism responsible for the recrystallization textures in $L1_2$-type ordered intermetallic alloys including the Co_3Ti and $Ni_3(Si,Ti)$ alloys, more studies are required.

B. *Twin Boundaries and Related Boundaries in $L1_2$-Ordered Intermetallic Alloys*

The recrystallized Co_3Ti and $Ni_3(Si,Ti)$ alloys contain a high frequency of $\Sigma 3$ boundaries, as has been similarly observed in recrystallized Ni_3Al.[39] Corresponding to this result, numerous annealing twins are observed in the recrystallized microstructures of these $L1_2$-type ordered intermetallic alloys. Particularly, the Co_3Ti alloys show a higher frequency of $\Sigma 3$ boundaries than the $Ni_3(Si,Ti)$ (and Ni_3Al) alloys.[39] For disordered fcc metals and alloys, it is known that the occurrence of annealing twins is related to stacking-fault energy (γ_{SFE}): annealing twins are formed in the recrystallized microstructures of fcc materials with a low or medium γ_{SFE}.[55] The stacking-fault energy of copper and aluminum has been reported to be $\sim$80 and $\sim$170 (mJm^{-2}), respectively.[56] However, the value of γ_{SFE} of the Co_3Ti and $Ni_3(Si,Ti)$ alloys is, unfortunately, not available at the present time.

Before estimating the value of γ_{SFE} of the Co_3Ti and $Ni_3(Si,Ti)$ alloys, we consider two planar faults, *i.e.*, the stacking fault and twin boundary on the {111} plane in $L1_2$-type ordered intermetallic alloys. For the stacking fault on the {111} plane, where the sequence *ABCABC* changes to the

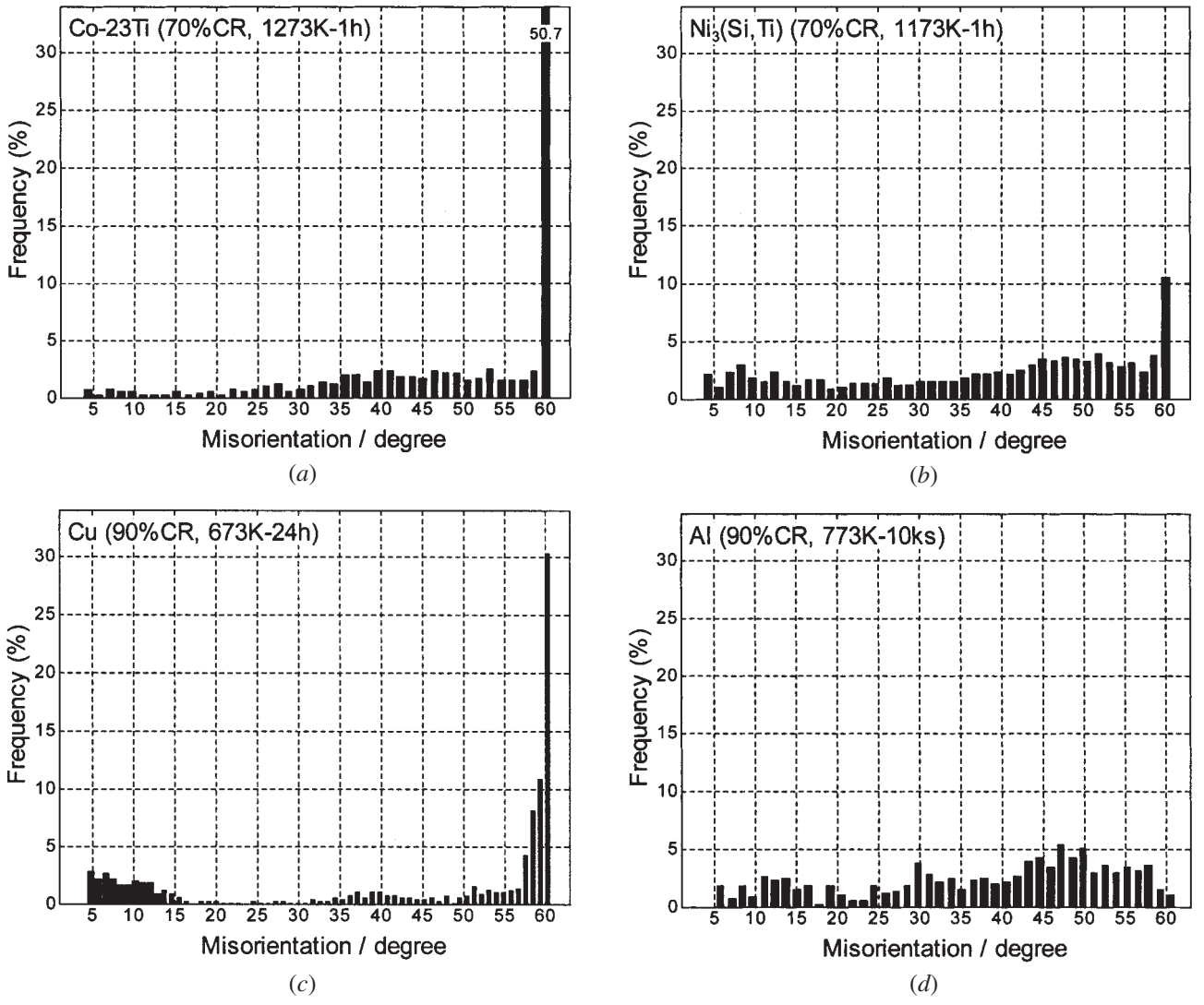

Fig. 5—Distribution of grain-boundary misorientation for the (*a*) Co-23 Ti, (*b*) $Ni_3(Si,Ti)$, (*c*) copper, and (*d*) aluminum. The annealing condition of each specimen is the same as that shown in Fig. 2.

sequence *ABCA*/*CAB*, three types of faults, *i.e.*, an antiphase boundary (APB), complex stacking fault (CSF), and superlattice intrinsic stacking fault (SISF) geometrically exist on the {111} plane.[57,58] The APB results from disturbance of unlike nearest neighbors and is a relatively high-energy fault. The CSF involving the nature of the SF and APB is a higher-energy fault than the SISF. The SISF results in a change in stacking sequence but with no nearest-neighbor violation and, thereby, is a lower-energy fault than the APB and CSF. Therefore, planar fault on the {111} plane of $L1_2$-type ordered intermetallic alloys is assumed to mainly exist as the SISF, if the energetic requirement operates. For a twin boundary on the {111} plane where the normal sequence of *ABCABC* changes to the reverse sequence *ABCA*/*CBA*, two types of faults, *i.e.*, the SISF and CSF, are geometrically possible, but the APB fault is geometrically impossible. It is deduced from the geometrical analysis that any twin-boundary structure always contains faulting for the sequence, but all twin-boundary structures do not always contain faulting for the bond, as has been actually argued in the previous study.[59,60] However, only the SISF is energetically favorable as a twin boundary on the {111} plane of $L1_2$-type ordered intermetallic alloys. Consequently, only the SISF-type fault is stable for not only a stacking fault, but also a twin boundary, on the {111} plane of $L1_2$-type ordered intermetallic alloys.

Now, let us estimate the stacking-fault energy or twin-boundary energy (γ_{twin}) of $L1_2(A_3B)$-type ordered intermetallic alloys. For both the stacking fault and twin boundary, the majority of bond pairs are A-A and they do not contain wrong (A-B) bond pairs because they are composed of the SISF type. Therefore, γ_{SFE} (or γ_{twin}) of $L1_2(A_3B)$-type ordered intermetallic alloys can be estimated as that of the major components, *i.e.*, A atoms: it follows that the γ_{SFE} of the Co_3Ti and $Ni_3(Si,Ti)$ alloys is close to that of fcc Co-(33 wt pct)Ni ($\sim$15 mJm^{-2}[61]) and of nickel ($\sim$130 mJm^{-2}[56]), respectively. Consequently, the value of γ_{SFE} can be ranked as of the order $Co_3Ti < Cu < Ni_3(Si,Ti) < Al$. The γ_{SFE} of the Co_3Ti alloy (or copper) is predicted to be lower than that of the $Ni_3(Si,Ti)$ (or Ni_3Al) alloy. This estimation is consistent with the fact that the observed annealing twins are more significant in the Co_3Ti alloys (or copper) than in the $Ni_3(Si,Ti)$ alloy (or Ni_3Al[39]). Thus, the value of γ_{SFE} is

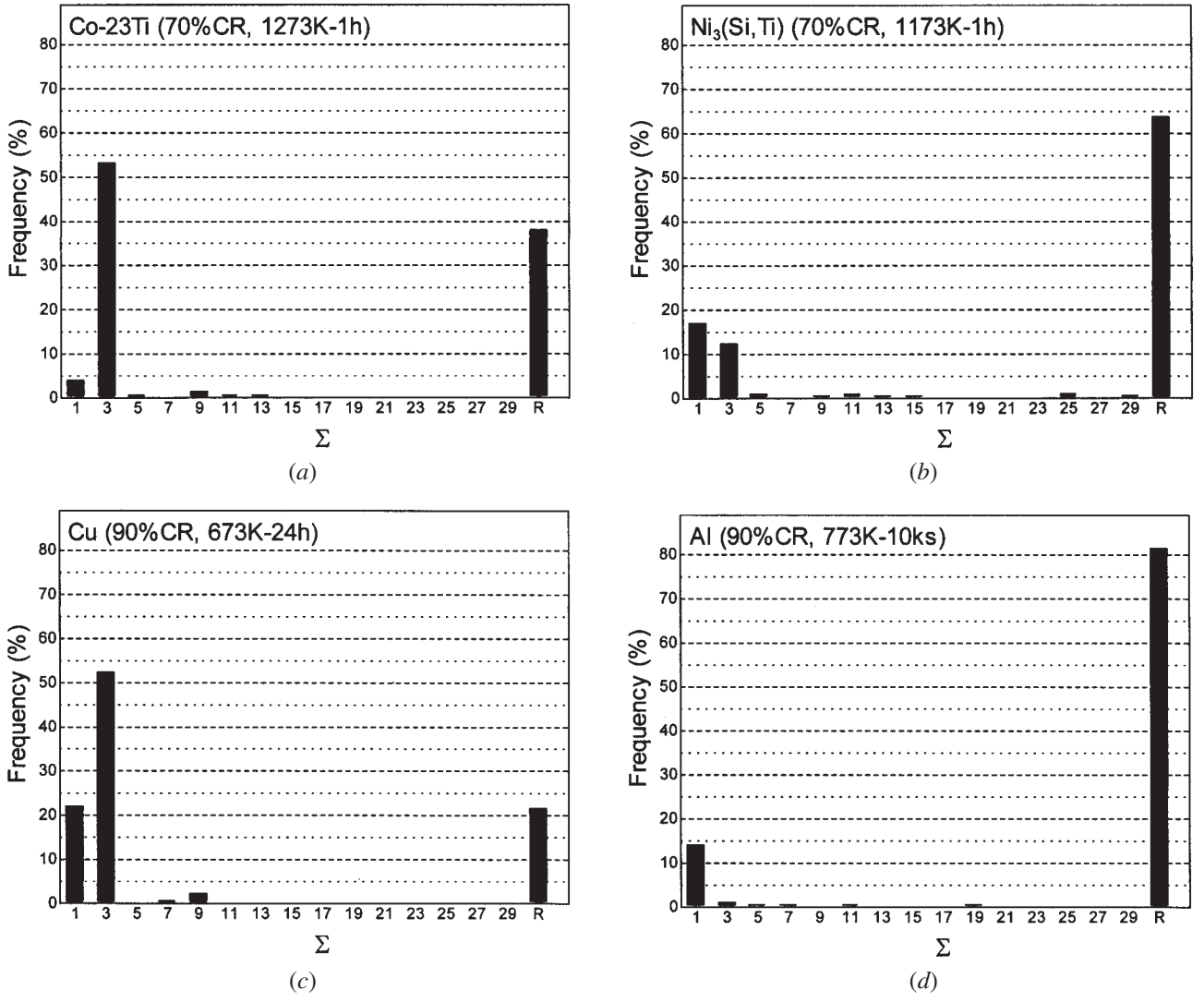

Fig. 6—Distribution of grain-boundary character for the (*a*) Co-23 Ti, (*b*) $Ni_3(Si,Ti)$, (*c*) copper, and (*d*) aluminum. The annealing condition of each specimen is the same as that shown in Fig. 2.

Table I. Summary of the GBCD

Material	Treatment	Low-Angle Boundaries (Pct)	Twin (and Related) Boundaries (Pct)			Other Coincidence Site Lattice Boundaries (Pct)	All Coincidence Site Lattice Boundaries (Pct)	Random Boundaries (Pct)
		Σ1	Σ3	Σ9	Σ27	Σ5-Σ7, Σ11-Σ25, Σ29	Σ1-Σ29	Σ > 29
Co-23 Ti	1273 K-1 h (30 pct CR)	4.7	47.0	2.1	0.3	2.9	57.0	43.0
	1273 K-1 h (50 pct CR)	4.9	45.8	1.7	0.3	3.5	56.2	43.8
	1273 K-1 h (70 pct CR)	3.8	53.1	1.6	0.2	3.2	61.9	38.1
$Ni_3(Si,Ti)$	1173 K-1 h (30 pct CR)	8.6	18.5	0.9	0.2	3.5	31.7	68.3
	1173 K-1 h (50 pct CR)	22.2	17.2	1.1	0.2	4.7	45.4	54.6
	1173 K-1 h (70 pct CR)	17.1	12.3	0.6	0.2	5.9	36.1	63.9
	1173 K-1 h (80 pct CR)	10.3	10.8	0.4	0.1	5.0	26.6	73.4
Cu	673 K-1 min (90 pct CR)	7.5	47.4	6.9	1.4	2.0	65.2	34.8
	673 K-15 min (90 pct CR)	12.6	48.6	5.7	1.5	1.8	70.2	29.8
	673 K-30 min (90 pct CR)	13.4	49.6	5.2	0.7	2.2	71.1	28.9
	673 K-2 h (90 pct CR)	17.4	46.4	3.5	0.6	1.2	69.1	30.9
	673 K-24 h (90 pct CR)	22.0	52.4	2.4	0.3	1.2	78.3	21.7
Al	773 K-1 s (90 pct CR)	12.7	3.1	0.6	0.2	6.5	23.1	76.9
	773 K-10 ks (90 pct CR)	14.2	1.2	0	0	3.3	18.7	81.3

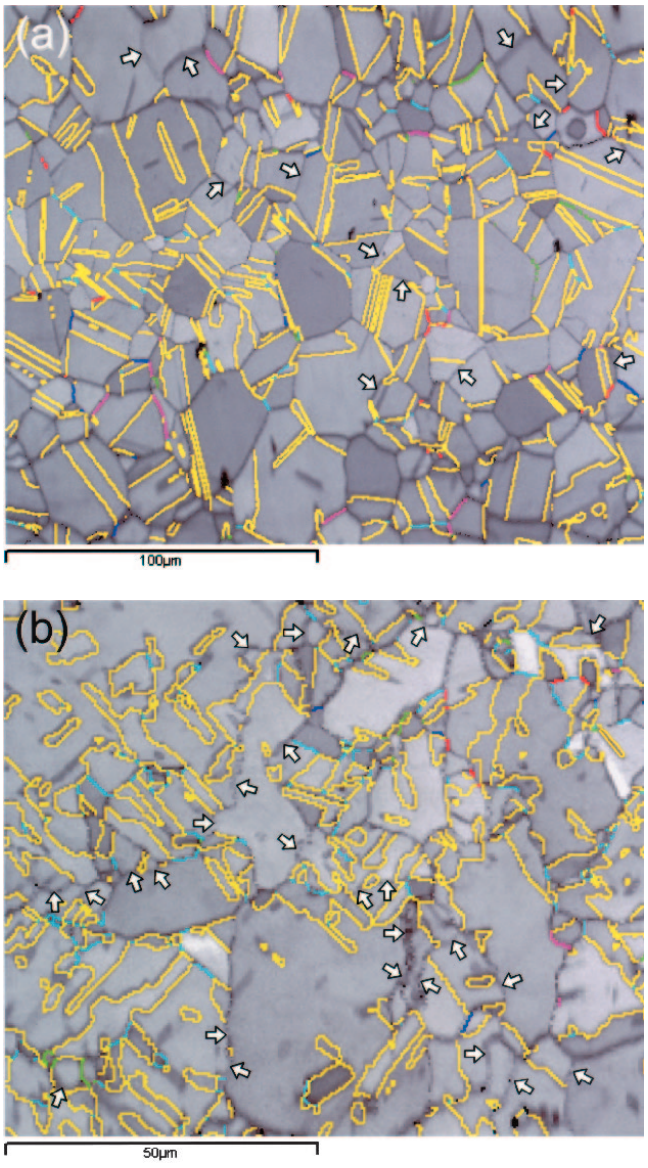

Fig. 7—EBSD boundary map for (*a*) Co-23 Ti that was cold rolled to 70 pct reduction and subsequently annealed at 1273 K for 1 h and (*b*) copper that was cold rolled to 90 pct reduction and subsequently annealed at 673 K for 1 h. The Σ3 and Σ9 boundaries are colored as yellow and light blue, respectively. Other low Σ boundaries are colored as red, purple, or green depending on the Σ value. Arrows indicate LABs, *i.e.*, Σ1 boundaries.

considered to be a prime factor affecting the frequency of annealing twins, regardless of disordered fcc materials or ordered $L1_2$ alloys.

As mentioned already, the SISF-type twin boundary (without involving the nature of the APB) is stable and has the least energy in an $L1_2$-type ordered intermetallic alloy. However, the geometrical argument indicates that most grain boundaries in an $L1_2$-type ordered intermetallic alloy generally involve the nature of a wrong bond, *i.e.*, APB.[58,59] In other words, grain boundaries in an $L1_2$-type ordered intermetallic alloy are generally composed of the CSF. Consequently, grain-boundary energy in an $L1_2$-type ordered intermetallic alloy can be expressed by the equation

$$\gamma_{GB} = \gamma(\theta) + \gamma^*(\theta) \quad [1]$$

where θ is the misorientation parameter defining the grain boundary, the first term is the energy only due to misorientation irrespective of ordered or disordered lattice, and the second term is due to the nature of the APB. Both terms are functions of the misorientation. The grain-boundary energy in disordered metals and alloys is composed of only the first term, while the grain-boundary energy in an $L1_2$-type ordered intermetallic alloy is composed of the two terms, except for the SISF-type twin boundary. As the misorientation parameter θ defines the grain boundary, there are, furthermore, some parameters: the Σ value, misorientation $\Delta\Theta$ (*i.e.*, deviation angle from an exact CSL relation), symmetric or asymmetric boundary plane, low- or high-index boundary plane, coherent or incoherent boundary plane, and so on. Generally describing, it is expected that as the Σ value increases, as $\Delta\Theta$ increases, or as the grain boundary changes from a symmetric to asymmetric plane, from a low- to high-index plane, or from a coherent to incoherent boundary, the contribution of the second term to Eq. [1] becomes larger.

These hypotheses are consistent with the two striking results observed in this study. The first result is that the morphological feature of the annealing twins is quite different between the Co_3Ti (and $Ni_3(Si,Ti)$) alloys and copper, although both materials similarly contain a high density of annealing twins. Relatively straight and long transgrain twin boundaries (*i.e.*, coherent twin boundaries) are occasionally observed in the Co_3Ti (and $Ni_3(Si,Ti)$) alloys, while numerous islandlike twins are observed in copper, accompanied by incoherent twin boundaries. In other words, it appears that incoherent twin boundaries hardly exist in the Co_3Ti (and $Ni_3(Si,Ti)$) alloys. This result indicates that the twin-boundary energy with a high-index plane (or an incoherent plane) is higher in an $L1_2$-type ordered intermetallic alloy than in disordered copper. The second result is that there is a distinctive difference in the GBCD between the Co_3Ti alloys and copper. It is apparent that the frequency of Σ9 and Σ27 boundaries is lower in the Co_3Ti alloys (and also in the $Ni_3(Si,Ti)$ alloy) than in copper, although the frequency of Σ3 boundaries is not so different between the Co_3Ti and copper (Table I). This result indicates that the grain-boundary energy of twin-related boundaries, *i.e.*, a high- Σ boundary such as Σ9 and Σ27, is higher in an $L1_2$-type ordered intermetallic alloy than in disordered copper. It is likely that the evolution (or transformation) from the Σ3 boundary to the Σ9 or Σ27 boundaries is retarded in an $L1_2$-type ordered intermetallic alloy because it has a high grain-boundary energy, although the kinetics for evolution may be concerned with this phenomenon.

V. CONCLUSIONS

The GBCD of the cold-rolled and recrystallized Co_3Ti and $Ni_3(Si,Ti)$ alloys with an $L1_2$ ordered structure was investigated along with copper and aluminum by means of the EBSD technique. The results obtained from the present study were as follows.

1. The GBCD of the Co_3Ti alloys was featured by a high frequency of Σ3 boundaries. On the other hand, the GBCD of the $Ni_3(Si,Ti)$ alloy was featured by a lower frequency of Σ3 and higher frequency of random (*e.g.*, $\Sigma \geq 29$) boundaries than that of the Co_3Ti alloys.

2. The recrystallization textures of both the Co_3Ti and $Ni_3(Si,Ti)$ alloys were considerably weak, but their GBCDs were similar to those of the pure copper and aluminum, which had a strong cube recrystallization texture, when $\Sigma 3$ boundaries are excluded from the evaluation by the GBCD.
3. The present results strongly suggest that the GBCD of the recrystallized Co_3Ti and $Ni_3(Si,Ti)$ alloys was dominated primarily by stacking-fault energy and secondarily by ordering energy.

REFERENCES

1. P.H. Humphrey: in *Grain Boundary Structure and Properties*, G.A. Chadwick and D.A. Smith, eds., Academic Press, London, 1976, pp. 139-200.
2. T. Watanabe: *Metall. Trans. A*, 1983, vol. 14, pp. 531-45.
3. L.C. Lim and T. Watanabe: *Acta Metall Mater*., 1990, vol. 38, pp. 2507-16.
4. M. Yamashita, S. Hashimoto, T. Mimaki, and S. Miura: *Mater. Trans*., 1991, vol. 32, pp. 885-97.
5. T. Watanabe: *Text. Microstr*., 1991, vols. 14–18, pp. 739-44.
6. A. Garbacz and M.W. Grabski: *Acta Metall. Mater*., 1993, vol. 41, pp. 469-73.
7. A. Garbacz and M.W. Grabski: *Acta Metall. Mater*., 1993, vol. 41, pp. 475-83.
8. D.C. Hinz and J.A. Szpunar: *Phys. Rev*., 1995, vol. B52, pp. 9900-09.
9. Y. Watanabe: *Proc. 11th Int. Conf. on Textures of Materials (ICOTOM-11)*, Z. Liang, L. Zuo, and Y. Chu, eds., International Academic Publishers, Beijing, 1996, pp. 1309-18.
10. E.A. Holm, G.N. Hassold, and M.A. Miodownik: *Acta Mater*., 2001, vol. 49, pp. 2981-91.
11. T. Watanabe, N. Yoshikawa, and S. Karashima: *Proc. Int. Conf. on Textures of Materials (ICOTOM-6)*, S. Nagashima, ed., The Iron and Steel Institute of Japan, Tokyo, 1981, pp. 609-18.
12. K. Matsumoto, T. Shibayanagi, and Y. Umakoshi: *Acta Mater*., 1997, vol. 45, pp. 439-51.
13. V. Randle, B. Ralph, and D. Dingley: *Acta Metall*., 1988, vol. 36, pp. 267-73.
14. J. Furly and V. Randle: *Mater. Sci. Technol*., 1991, vol. 7, pp. 12-19.
15. W.E. King and A.J. Schwartz: *Scripta Mater*., 1998, vol. 38, pp. 449-55.
16. O.V. Mishin: *Scripta Mater*., 1998, vol. 38, pp. 423-28.
17. O.V. Mishin and G. Gottstein: *Mater. Sci. Eng. A*, 1998, vol. 249, pp. 71-78.
18. T. Watanabe, H. Fujii, H. Okikawa, and K.I. Arai: *Acta Metall*., 1989, vol. 37, pp. 941-52.
19. K. Aoki and O. Izumi: *J. Jpn. Inst. Met*., 1979, vol. 43, pp. 1190-96.
20. T. Takasugi and O. Izumi: *Acta Metall*., 1985, vol. 33, pp. 39-48.
21. T. Takasugi, M. Nagashima, and O. Izumi: *Acta Metall. Mater*., 1990, vol. 38, pp. 747-55.
22. G. Gottstein, P. Nagpal, and W. Kim: *Mater. Sci. Eng. A*, 1989, vol. 108, pp. 165-79.
23. J. Ball and G. Gottstein: *Intermetallics*, 1993, vol. 1, pp. 171-85.
24. J. Ball and G. Gottstein: *Intermetallics*, 1993, vol. 1, pp. 191-208.
25. C. Escher, S. Neves, and G. Gottstein: *Acta Mater*., 1998, vol. 46, pp. 441-50.
26. S.G. Chowdhury, R.K. Ray, and A.K. Jena: *Mater. Sci. Eng. A*, 2000, vol. 277, pp. 1-10.
27. B. Bhattacharya and R.K. Ray: *Metall. Mater. Trans. A*, 2000, vol. 31, pp. 3011-21.
28. T. Takasugi and O. Izumi: *Acta Metall*., 1985, vol. 33, pp. 49-58.
29. H.Y. Yasuda, S. Yamamura, and Y. Umakoshi: *Scripta Mater*., 2001, vol. 44, pp. 765-69.
30. Y. Kaneno, I. Nakaaki and T. Takasugi: *J. Mater. Res*., 2002, vol. 17, pp. 2567-77.
31. T. Takasugi, S. Rikukawa, and S. Hanada: *Acta Metall. Mater*., 1992, vol. 40, pp. 1895-1906.
32. Y. Kaneno, M. Wada, H. Inoue, and T. Takasugi: *Mater. Trans*., 2001, vol. 42, pp. 418-21.
33. Y. Kaneno, I. Nakaaki, and T. Takasugi: *Intermetallics*, 2002, vol. 10, pp. 693-700.
34. M. Demura, Y. Suga, O. Umezawa, K. Kishida, E.P. George, and T. Hirano: *Intermetallics*, 2001, vol. 9, pp. 157-67.
35. S. Hanada, T. Ogura, S. Watanabe, O. Izumi, and T. Masumoto: *Acta Metall*., 1986, vol. 34, pp. 13-21.
36. H. Liu and D.P. Pope: *Acta Metall. Mater*., 1993, vol. 41, pp. 553-62.
37. T. Watanabe, T. Hirano, T. Ochiai, and H. Oikawa: *Mater. Sci. Forum*, 1994, vol. 157-162, pp. 1103-08.
38. H. Lin and D.P. Pope: *Mater. Sci. Eng. A*, 1995, vols. 192-93, pp. 394-98.
39. N. Masahashi and S. Hanada: *Z. Metallkd*., 2000, vol. 91, pp. 516-22.
40. L.C.R. Lopes: *Scripta Mater*., 1997, vol. 37, pp. 1863-68.
41. I. Samajdar, P. Ratchev, B. Verlinden, and D. Schryvers: *Intermetallics*, 1998, vol. 6, pp. 419-25.
42. J. Bystrzycki, R.A. Varin, M. Nowell, and K.L. Kurzydlowski: *Intermetallics*, 2000, vol. 8, pp. 1049-59.
43. D.G. Brandon: *Acta Metall*. 1966, vol. 12, pp. 1479-84.
44. W.G. Burgers: *Recrystallization, Grain Growth and Textures*, ASM, Metals Park, OH, 1965, p. 128.
45. R.D. Doherty: in *Recrystallization of Metallic Materials*, F. Haessner, ed., Dr. Riederer Verlag GmbH, Stuttgart, 1978, p. 124.
46. H. Mecking: in *Preferred Orientation in Deformed Metals and Rocks: An Introduction to Modern Texture Analysis*, H.R. Wenk, ed., Academic Press, Orlando, FL, 1985, p. 298.
47. F.J. Humphreys and M. Hatherly: *Recrystallization and Related Annealing Phenomena*, Elsevier Science, Oxford, United Kingdom, 1995, p. 44.
48. K. Ito, R. Musick, and K. Lücke: *Acta Metall*., 1983, vol. 31, pp. 2137-49.
49. K. Ito, F. Seki, H. Abe, and K. Lücke: *Z. Metallkd*., 1983, vol. 74, pp. 772-76.
50. J. Hirsch and Lücke: *Acta Metall*., 1985, vol. 33, pp. 1927-38.
51. J.K. Mackenzie: *Acta Metall*., 1964, vol. 12, pp. 223-25.
52. C. Davies and V. Randle: *Mater. Sci. Technol*., 2001, vol. 17, pp. 615-26.
53. W.B. Hutchinson, F.M.C. Besag, and C.V. Honess: *Acta Metall*., 1973, vol. 21, pp. 1685-91.
54. A.A. Ridha and W.B. Hutchinson: *Acta Metall*., 1982, vol. 30, pp. 1929-39.
55. L.E. Murr: *Interfacial Phenomena in Metals and Alloys*, Addison-Wesley, Reading, MA, 1975, pp. 219-21.
56. *Interfacial Phenomena in Metals and Alloys*, Addisong-Wesley, Reading, MA, 1975, pp. 145-48.
57. M. Yamaguchi and Y. Umakoshi: *Progr. Mater. Sci*., 1990, vol. 34, pp. 1-148.
58. N.S. Stoloff and C.T. Liu: in *Physical Metallurgy and Processing of Intermetallic Compounds*, N.S. Stoloff and V.K. Sikka, eds., Chapman and Hall, New York, NY, 1996, pp. 164-66.
59. T. Takasugi and O. Izumi: *Acta Metall*., 1983, vol. 31, pp. 1187-1202.
60. T. Takasugi and O. Izumi: *Acta Metall*., 1987, vol. 35, pp. 823-33.
61. T. Ericsson: *Acta Metall*., 1966, vol. 14, pp. 853-65.